Supporting Information

Superionic conduction along ordered hydroxyl networks in molecular-thin nanosheets

Pengzhan Sun,†[a,b] Fashen Chen,†[a,c] Wei Zhou,[d] Xiaohe Liu, *[c] Renzhi Ma,*[a] and Takayoshi Sasaki[a]

[a] *World Premier International Center for Materials Nanoarchitectonics (WPI-MANA), National Institute for Materials Science (NIMS), 1-1 Namiki, Tsukuba, Ibaraki 305-0044, Japan. E-mail: MA.Renzhi@nims.go.jp*
[b] *School of Physics and Astronomy, University of Manchester, Manchester M13 9PL, UK.*
[c] *State Key Laboratory of Powder Metallurgy, School of Materials Science and Engineering, Central South University, Changsha, Hunan 410083, China. E-mail: liuxh@csu.edu.cn*
[d] *TU-NIMS International Collaboration Laboratory, School of Material Science and Engineering, Tianjin University, Tianjin 300072, China.*
† These authors contributed equally to this work.

1. Supplementary Materials and Methods

1.1 Preparation of Mg-Al and Co-Al LDH nanosheets.

Well-crystallized hexagonal-shaped LDH precursors containing various divalent/trivalent heterogeneous metal cations (*e.g.* Mg-Al-LDH and Co-Al-LDH) were synthesized through well-established soft-chemical routes.[1,2] Briefly, Mg-Al-CO_3^{2-} LDH precursors ($Mg_{2/3}Al_{1/3}(OH)_2(CO_3)_{1/6}\cdot 0.5H_2O$) were synthesized *via* hexamethylenetetramine (HMT, $C_6H_{12}N_4$) hydrolysis of a mixed solution of $Mg(NO_3)_2\cdot 6H_2O$ and $Al(NO_3)_3\cdot 9H_2O$ (Mg/Al ratio of 2) by hydrothermal treatment. Co-Al-CO_3^{2-} LDH precursors ($Co_{2/3}Al_{1/3}(OH)_2(CO_3)_{1/6}\cdot 0.5H_2O$) were synthesized *via* urea ($CO(NH_2)_2$) hydrolysis of a mixed solution of $CoCl_2\cdot 6H_2O$ and $AlCl_3\cdot 6H_2O$ (Co/Al ratio of 2) by refluxing. The as-synthesized powders were washed, collected and subjected to decarbonation and anion exchange to adjust the interlayer ions from CO_3^{2-} to NO_3^- by mechanical shaking in a mixed salt-acid solution containing $NaNO_3$ and HNO_3. Finally, delamination/exfoliation of Mg-Al-NO_3^- and Co-Al-NO_3^- LDH crystals was achieved by mechanical shaking in formamide.

1.2 Fabrication of electrical contacts on selected individual nanosheets.

Si/SiO_2 (300 nm) wafers were first immersed in HCl/methanol (1:1 in volume) mixed solution for 30 min, followed by concentrated H_2SO_4 for 30 min to remove contaminates and make the surfaces hydrophilic. Then the wafers were thoroughly washed with water and dipped into Mg-Al (or Co-Al) LDH nanosheet formamide dispersion (0.01 mg/mL), immediately taken out and rinsed with abundant water to deposit nanosheets discretely and sparsely. The wafers were blow dried. Bilayer PMMA (3%, 495 / 3%, 950) was spin-coated on the nanosheet-containing wafers. A mask for depositing electrical contacts on selected individual sheet was made by standard e-beam lithography. Au (60 nm) /Cr (4 nm) was deposited onto the mask using e-beam evaporator, followed by lifted off in hot acetone (80 ^oC). Then the samples were washed thoroughly with fresh acetone and IPA and blow dried.

1.3 Measurements of hydroxide ion conductivity.

Before measurements, silver wires were introduced from the electrical contacts on individual nanosheets with the assistance of silver paste under microscope. In this step, hands should be grounded. A.C. impedance spectrum was acquired with an LCR meter (6500P WAYNE KERR, frequency range: 20 Hz ~ 10 MHz) in a constant temperature and humidity chamber (IW 223 Yamato Scientific Co., LTD), which was then transferred to the Z-plot/Z-view software package (Scribner Associates). By fitting the spectrum into semicircle (the associated fitting uncertainty in software did not exceed 1%, which was negligible), ion conducting resistance (R) was determined from the intersection of the low-frequency end of fitted semicircle with the real axis. Hydroxide ion conductivity (σ) was then calculated by taking the geometric parameters into consideration ($\sigma = W/(R \times t \times L)$, where W is the width of nanosheet connecting two electrodes, t is the nanosheet thickness: 0.48 nm of crystallographic thickness and ~1 nm of actual AFM-measured thickness, both cases were considered, L is the nanosheet length, Fig. 1B).

1.4 Ab initio density functional theory-based simulations.

All calculations were performed using Vienna *ab initio* package (VASP) based on the density functional theory.[3] Generalized gradient approximation (GGA) was used for the exchange-correlation energy. D2

method prosed by Grimme was adopted to describe the van der Waals interactions.[4] A plane-wave expansion for the basis was set with a cutoff energy of 400 eV. A vacuum region of 18 Å was used to eliminate interactions between the neighboring cells of slab models. 2×2×1 Monk-horst *k*-point meshes were used for the Brillouin-zone integrations of slab supercell models. All atoms in the equilibrium structures were relaxed until the total energy difference and residual force were less than 1×10^{-5} eV and 0.01 eV/Å, respectively. For the explicit model with multiple water molecule coverage, two layers with 12 water molecules in total were added above one side of Mg-Al LDH single-layer sheet, which corresponded to 50% of surface coverage. For the analysis of charge transfer in the formation of hydrogen bond, Bader charge model was taken into account.[5] In addition, the climbing-image nudged elastic band (CI-NEB) method was employed to estimate the reaction and diffusion barriers.[6] Nine images along the reaction pathway were used between the fixed endpoints and the spring constant was set to -5 eV/Å^2. The energy and force criteria for CI-NEB calculations were 1×10^{-5} eV and 0.02 eV/Å, respectively. The transition states were confirmed with only one imaginary vibrational mode by performing frequency analysis.

1.5 Calculation of activation energy

The activation energy (E) of hydroxide ion conduction was calculated from:

$$\sigma T = Aexp(-\frac{E}{k_B T})$$

A is the Arrhenius factor and k_B is the Boltzmann constant. E could be obtained from the slope of linear fit for ln (σT) *versus* T^{-1}.

1.6 pH measurements of nanosheet aqueous dispersion

In order to quantitatively evaluate the ability of free hydroxide ion production by the LDH-water system, freshly exfoliated Mg-Al LDH nanosheets were collected *via* centrifugation and repeatedly washed with ethanol. After freeze-dried to remove residual solvent, 16 mg of Mg-Al LDH nanosheets were dispersed in 10 mL of water *via* sonication and pH of the mixture was measured under vigorous stirring. More

water (20 mL for each step) was gradually added into the dispersion and pH was measured continuously under stirring (fully stirred for 40 min before each measurement). Three identical runs were performed. The results are shown in Fig. S3.

Since LDH nanosheets were exfoliated in formamide, the surface adsorption of formamide molecules might affect the pH measurements of nanosheet dispersions. In order to quantitatively estimate the effect of formamide, it is assumed that single-layer formamide molecules are densely adsorbed on nanosheet surfaces instead of water molecules, which serves as an upper bound estimation.

First, the total surface area of certain amount of Mg-Al LDH nanosheets is estimated. The area of in-plane unit cell can be calculated as $S_0 = a^2\sin\alpha$ (a is the in-plane lattice constant, 0.3 nm and α is the included angle between two base axes, 120°). Therefore, the total surface area of Mg-Al LDH nanosheets with a mass of m (g) can be estimated as $S = 2N_A S_0 m/M$, where M is the molar mass of Mg-Al LDHs, $Mg_{2/3}Al_{1/3}(OH)_2(NO_3)_{1/3}\cdot 0.5H_2O$, ~88.9 g/mol.

Assume an individual formamide molecule can be treated as a ball. Its volume can be estimated as $V_f = M_f/(\rho N_A)$, where M_f is the molar mass of formamide (CH_3NO, 45.04 g/mol) and ρ is the density of formamide liquid at normal pressure and temperature (1.13 g/cm^3). Therefore, the radius (r) of the molecule can be extracted from $V_f = 4/3\pi r^3$. The total equivalent volume of formamide molecules adsorbed on nanosheet surfaces can be estimated as $V = M_f S/(\rho N_A \pi r^2)$. For 16 mg of Mg-Al LDH nanosheets, the estimated volume of formamide molecules adsorbed on nanosheet surfaces was ~6 μL.

We gradually added the same amount of water as that in nanosheet case into 6 μL and 0.6 mL formamide, which are comparable to and 2 orders of magnitude more than the estimated upper bound for the total volume of nanosheet surface adsorbed molecules, respectively, and monitored the pH variations. The results are shown in Fig. S4, revealing the negligible effect of formamide residual on pH measurements of LDH nanosheet dispersions.

1.7 Evaluation of hydroxide ion mobility along LDH hydroxyl slabs

At room temperature, the ratio of free hydroxide ions produced from hydrolysis of hydroxyl slabs was estimated as 0.5%~1.1% based on the densities of hydroxide ions and LDH-bearing hydroxyl groups in dispersions, which contained 16 mg of Mg-Al LDH nanosheets and 70~150 mL of water. The data plots used for estimation are marked with green square in Fig. S3B. The molar mass of Mg-Al LDH nanosheet was taken from its corresponding chemical formula of bulk precursor, $Mg_{2/3}Al_{1/3}(OH)_2(NO_3)_{1/3}\cdot 0.5H_2O$, ~88.9 g mol^{-1}.

Considering the crystal structure of LDH single-layer sheet, the distance between adjacent hydroxyl groups (a) is 0.3 nm and the thickness (t) is 0.48 nm. This yields a hydroxyl group numerical density on LDH single-layer sheet of ~5.3×10^{28} m^{-3}, if two hydroxyl slab surfaces are taken into account ($n_0 = 2/(a^2 t \sin\alpha)$). Actually, in our nanosheet-on-substrate device structure, where only one side was accessible to water molecules around, it is more plausible to consider one hydroxyl slab surface involved in hydroxide ion conduction. In this case, the hydroxyl group numerical density would be half of the above value ($n_0' = 1/(a^2 t \sin\alpha)$), ~$2.7 \times 10^{28}$ m^{-3}. Therefore, the concentration of free hydroxide ions produced from LDH-water system could be estimated as n_{OH} = 0.5%~1.1% n_0'. If the hydroxide ion conductivity of LDH single-layer sheets at 90% RH and room temperature (σ, ~0.15 S cm^{-1} for 0.48 nm of crystallographic thickness, Fig. 1D, and ~0.07 S cm^{-1} for ~1 nm of actual thickness) was taken into consideration, the mobility could be estimated as $\mu = \sigma/n_{OH}e$ = 1.5~6.9×10^{-7} m^2 V^{-1} s^{-1}. Note that this is a lower bound estimation since at 90% RH n_{OH} should be lower than that in liquid water.

1.8 Isotope effects

In order to seek if the hydroxyl slabs on covalently-bonded LDH single-layer sheets were involved in the conduction process, as-exfoliated Mg-Al LDH nanosheets were first collected through centrifugation and washed with ethanol for several times, freeze-dried to remove residual solvent and calcined at 200 ^oC for 1 h to get rid of possible crystal water. Then the nanosheet samples were re-dispersed in D_2O by sonication and stirred at room temperature or 80 ^oC for 24 h. Finally, the samples were freeze-dried and calcined again at 200 ^oC for 1 h to get rid of possible crystal water. Fourier

Transform infrared (FTIR) spectrum was acquired for each step to confirm the possible existence of isotope substituted hydroxyl groups (–OD).

Fig. S7A shows FTIR spectra for each step of treatment (pristine, first calcination at 200 ^{o}C for 1 h, stirring in D_2O for 24 h and freeze-drying, second calcination at 200 ^{o}C for 1 h), which were baselined and normalized with the intensity of the peak at ~3340 cm^{-1} (assigned to –OH). Comparing with the pristine case and samples after the first calcination, a new peak located at ~2500 cm^{-1} emerged after being stirred in D_2O and freeze-dried, which could be attributed to the extension vibration mode of –OD. This indicates the presence of –OD groups or D_2O on LDH basal planes. After the second calcination, whereby 200 ^{o}C was believed to be enough for the removal of crystal water, the peak located at ~2500 cm^{-1} was still present with a relatively weaker intensity, further confirming the existence of –OD groups on LDH host layers. We also attempted to exchange the as-collected LDH nanosheets in D_2O with an elevated temperature (80 ^{o}C) and acquired FTIR spectra before and after the second calcination (Figs. S7B, C). It is seen that the normalized intensity of the peak at ~2500 cm^{-1} was stronger than that at room temperature for both cases, indicating that higher temperature promoted the isotope substitution of hydroxyl groups on LDH host layers. These results serve as an evidence for the participation of hydroxyl slabs in the concerted hydroxide ion conduction.

1.9 Evaluation of hydroxide ion conductivity through individual hydroxyl slit

Ion conducting resistance (R) was acquired as a function of RH and temperature for the LDH nanosheet junction devices, from which $\sigma \times t$ ($\sigma \times t = W/(R \times L)$ to include the complex junction thickness t) was calculated (Fig. S8). Comparing with the single-layer case, $\sigma \times t$ values for the junction-containing devices were slightly higher, showing the contribution from interlayer slit to the overall hydroxide ion conduction. In view of the structure of overlapped LDH nanosheet junction on substrate, it could be decomposed into one hydroxyl top surface with one individual hydroxyl slit. The hydroxyl top surface could be further equivalent to one LDH single-layer sheet. Therefore, hydroxide ion conduction across the junction could be equivalent to either through the individual slit or along the nanosheet surface (*i.e.*

R_{sl} and R_j in parallel, the subscript "sl" refers to single layer, "j" refers to junction slit). $R = W/(\sigma \times t \times L)$, where W is the width of single-layer or junction parts, t is the single-layer thickness (0.48 nm) or the junction interlayer spacing (~1.1 nm obtained from XRD of multilayer nanosheet stacking, Ref. 7), L is the length of single-layer or junction parts. In order to calculate the ion conducting resistance of single-layer parts (R_{sl}), the conductivity (σ) of single-layer sheets in Fig. 1D was put into the equation $R = W/(\sigma \times t \times L)$. The overall conducting resistance could be obtained from A.C. impedance spectrum of LDH nanosheet junction device. Therefore, the conducting resistance through individual slit from two narrowly stacked LDH single-layer sheets (R_j) could be extracted from the corresponding equivalent circuits in Figs. 4 and S9, based on which the hydroxyl slit conductivity could be calculated using $\sigma = W/(R \times t \times L)$.

2. Supplementary Figures

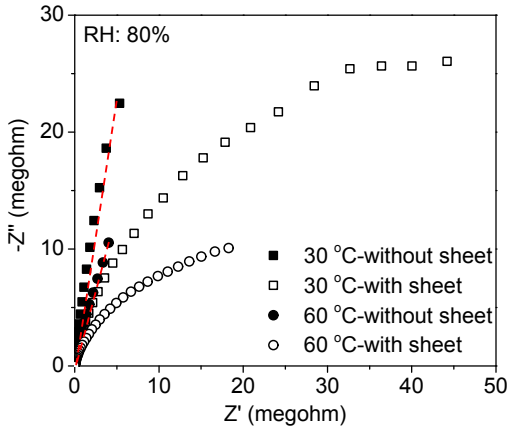

Fig. S1 A.C. impedance spectra of dummy device with electrical contacts made on blank Si/SiO_2 wafer. The spectra for electrical contacts made on LDH single-layer sheet are shown for comparison. RH: 80%, temperature: 30 °C and 60 °C. Dashed lines are linear fits to the plots for the dummy device.

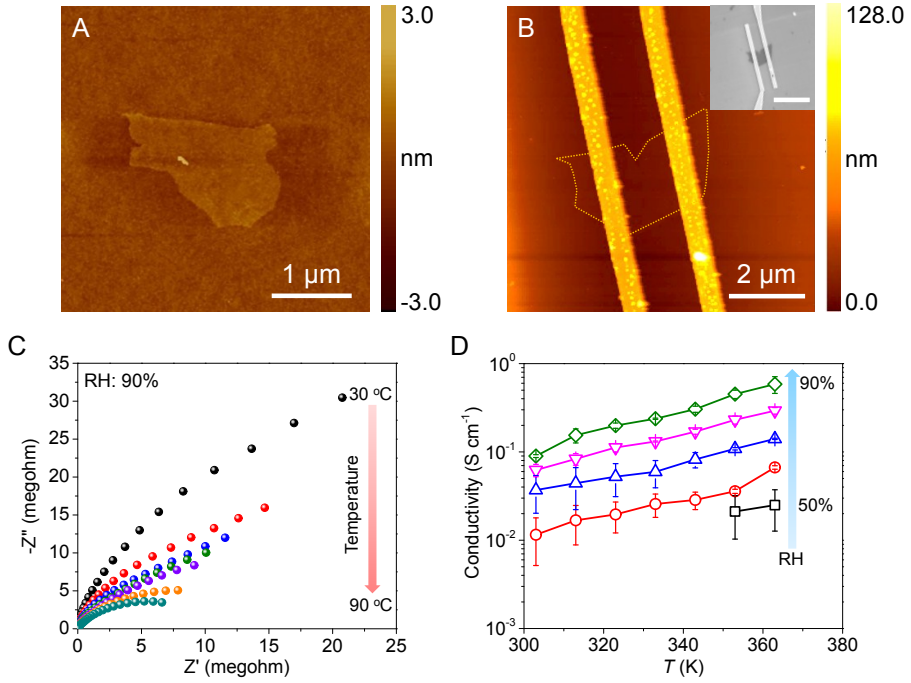

Fig. S2 Hydroxide ion conduction in Co-Al LDH single-layer sheets. (A) AFM image of Co-Al LDH single-layer sheet on Si/SiO_2 substrate. (B) AFM characterization of Co-Al LDH single-layer device. The dashed pattern outlines the nanosheet. Inset shows corresponding SEM image. Scale bar: 5 μm. (C) Representative A.C. impedance spectra of individual Co-Al LDH single-layer sheet acquired at 90% RH and 30~90 °C. (D) Temperature-dependent hydroxide ion conductivities of individual Co-Al LDH single-layer sheets at 50%~90% RH. The error bars in (D) are standard deviations based on at least three devices.

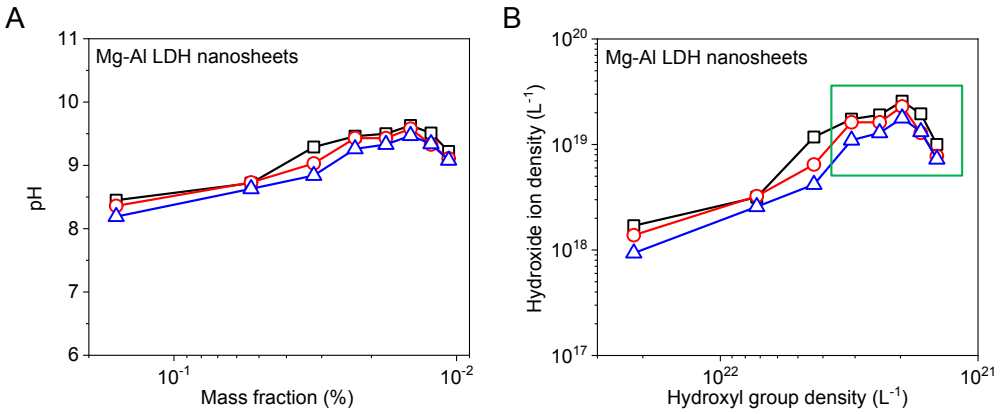

Fig. S3 pH measurements of nanosheet aqueous dispersions. (A) pH values of Mg-Al LDH nanosheet aqueous dispersions as a function of mass fraction. (B) Corresponding density of hydroxide ions as a

function of the density of LDH sheet-bearing hydroxyl groups in dispersions. The data plots used for estimating the ratio of free hydroxide ions produced from hydrolysis of hydroxyl slabs are marked with green square. Three runs were performed and different shaped plots represent different runs.

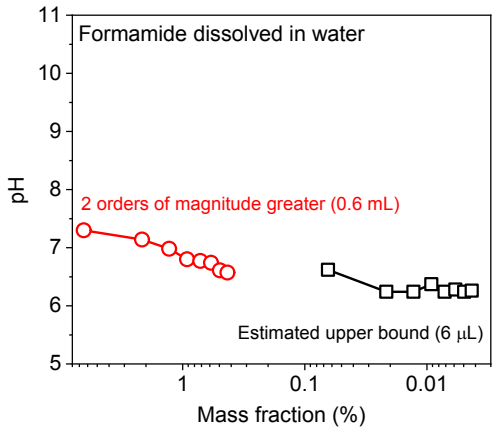

Fig. S4 Effect of formamide residue on pH measurements. pH values of aqueous solutions containing 6 μL and 0.6 mL formamide, which are comparable to and 2 orders of magnitude more than the estimated upper bound for the total volume of nanosheet (16 mg) surface adsorbed molecules, respectively, as a function of mass fraction.

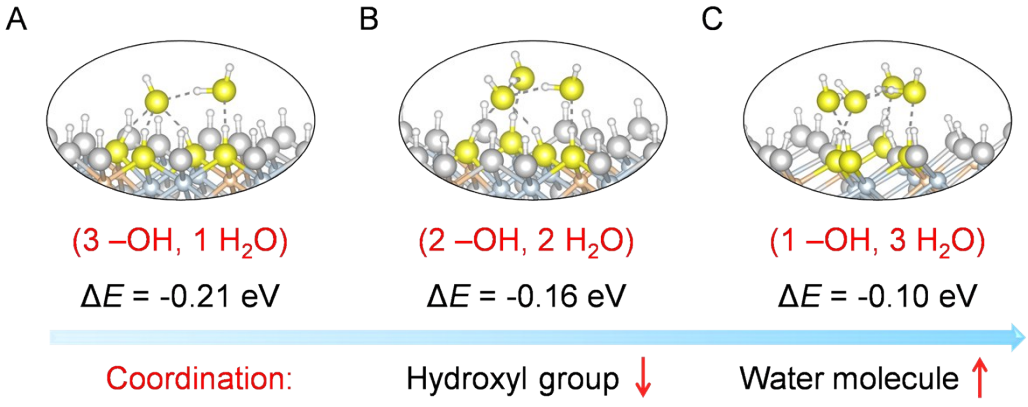

Fig. S5 Representative hydroxide ion solvation configurations with varying hydrogen-bonded hydroxyl group and water molecule numbers. Hydroxide ion coordinated with (A) 3 hydroxyl groups and 1 water molecule, (B) 2 hydroxyl groups and 2 water molecules, (C) 1 hydroxyl group and 3 water molecules. The energy difference between free hydroxide ion coordinating with hydroxyl group and water molecule ($\Delta E = E_{\text{hydroxyl}} - E_{\text{water}}$) was calculated and shown below each configuration. Silver, white,

light blue and orange balls denote oxygen, hydrogen, divalent and trivalent metal atoms, respectively. Specially, yellow balls denote the oxygen atoms involved in coordination.

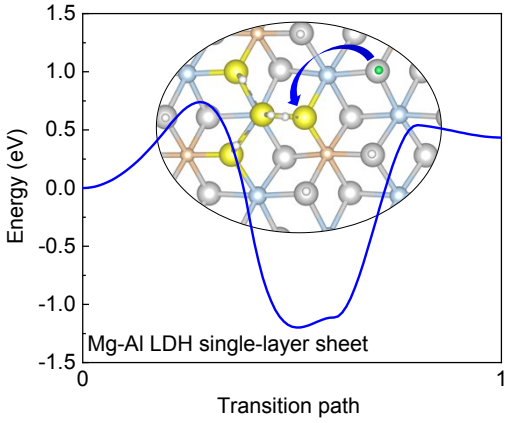

Fig. S6 The simulated energy profile for proton transfer between adjacent hydroxyl groups on Mg-Al LDH single-layer sheet. The inset shows a schematic diagram. After a proton on hydroxyl group was transferred whereby a proton "vacancy" was produced, a new transfer event from adjacent hydroxyl group to the vacancy was triggered. Specially, the green ball denotes the transferred proton.

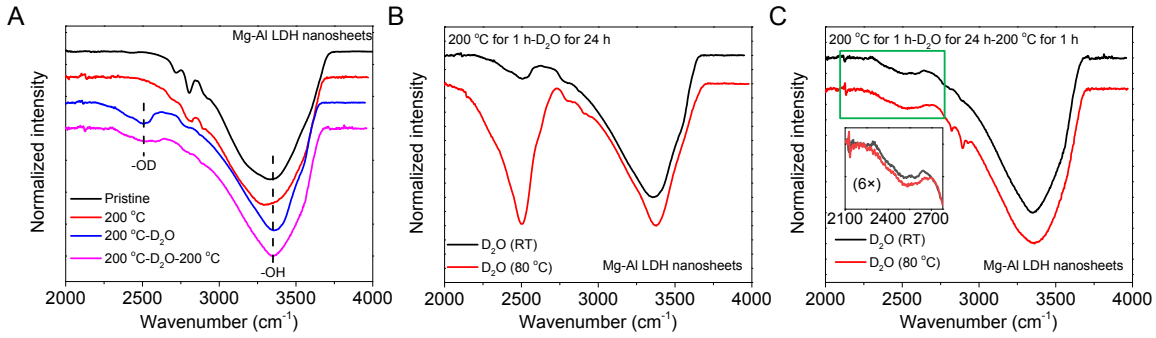

Fig. S7 FTIR spectra of nanosheets exchanged in D_2O. (A) FTIR spectra of Mg-Al LDH nanosheets after each step of treatment (pristine, first calcination at 200 °C for 1 h, stirring in D_2O for 24 h and freeze-drying, second calcination at 200 °C for 1 h). (B) and (C) FTIR spectra of Mg-Al LDH nanosheets after stirring in D_2O at room temperature and 80 °C, respectively. (B) Samples were calcined at 200 °C for 1 h, stirred in D_2O for 24 h and freeze-dried before FTIR measurements. (C) Samples were calcined at 200 °C for 1 h, stirred in D_2O for 24 h, freeze-dried and calcined again at 200 °C for 1 h

before FTIR measurements. The inset in (C) shows an enlarged view (6×) of the region marked with green square.

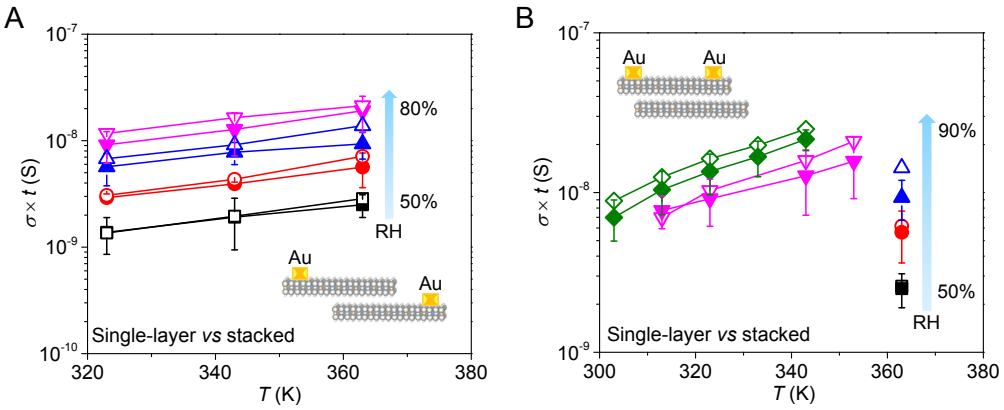

Fig. S8 Temperature-dependent $\sigma \times t$ ($\sigma \times t = W/(R \times L)$) of the nanosheet junction devices at various RHs. (A) Electrical contacts were introduced on each single-layer part leaving the junction in between. (B) Electrical contacts were directly made on the junction. Empty symbols are data for nanosheet junction devices and solid symbols are for single-layer devices calculated from Fig. 1D. Schematics for the junction device structures are shown in the insets.

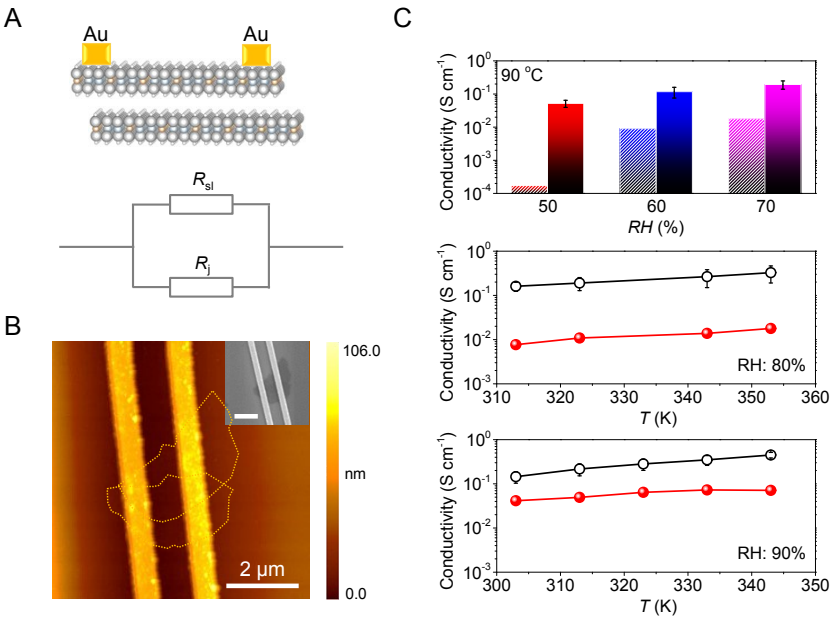

Fig. S9 Hydroxide ion conduction in nanosheet junction device with electrical contacts directly made on the junction. (A) Schematic for the device structure and corresponding equivalent circuit. (B) AFM

image of the Mg-Al LDH nanosheet junction device. Dashed patterns outline the overlapped nanosheets. Corresponding SEM image is shown in the inset. Scale bar: 2 μm. (C) Top panel: at 90 °C, the individual hydroxyl slit conductivities at 50%~70% RH extracted from the equivalent circuit in (A) (shaded bars on the left) as compared with those of surface conduction taken from Fig. 1D (solid bars on the right). Middle and bottom panels: temperature-dependent individual hydroxyl slit conductivities at 80% and 90% RH (solid symbols), respectively, as compared with the corresponding data for surface conduction taken from Fig. 1D (hollow symbols).

References

[1] L. Li, R. Ma, Y. Ebina, N. Iyi and T. Sasaki, *Chem. Mater.* 2005, **17**, 4386–4391.

[2] Z. Liu, R. Ma, M. Osada, N. Iyi, Y. Ebina, K. Takada and T. Sasaki, *J. Am. Chem. Soc.* 2006, **128**, 4872–4880.

[3] G. Kresse and J. Furthmüller, *Comput. Mater. Sci.* 1996, **6**, 15–50.

[4] S. J. Grimme, *Comput. Chem.* 2006, **85**, 1787–1799.

[5] G. Henkelman, A. Arnaldsson and H. Jónsson, *Comput. Mater. Sci.* 2006, **36**, 354–360.

[6] G. Henkelman and H. Jónsson, *J. Chem. Phys.* 2000, **113**, 9901–9904.

[7] P. Sun, R. Ma, X. Bai, K. Wang, H. Zhu and T. Sasaki, *Sci. Adv.* **2017**, **3**, e1602629.